2024 European Control Conference (ECC)
June 25-28, 2024. Stockholm, Sweden

$\mathcal{H}_\infty$ control experiments for increasing H_2 purity in high-pressure alkaline electrolyzers

Martín David, Fernando D. Bianchi, Carlos Ocampo-Martinez, *Senior Member, IEEE*, and Ricardo Sánchez-Peña, *Senior Member, IEEE*

***Abstract*— In this paper, an $\mathcal{H}_\infty$ control strategy is implemented in a prototype alkaline electrolyzer to maintain equalized the liquid levels in the separations chambers while following a pressure reference. The aim is to minimize the contamination of the gases produced by the electrolyzer. To this end, two outlet valves are controlled in the output lines of both gases: H_2 and O_2. The performance of the proposed control strategy was experimentally evaluated under different operating conditions. In all cases, H_2 contamination in O_2 was below 0.2%.**

I. Introduction

The hydrogen economy has been proposed as a comprehensive solution to store and supply energy originally produced from renewable sources [1], [2]. In this sense, electrolysis appears as a direct way of transforming electrical energy from renewable sources into chemical energy in the form of hydrogen molecules, which can later be used in fuel cells or engines [3]. In particular, the alkaline electrolysis studied here consists in the separation of water into oxygen and hydrogen molecules in an alkaline medium, usually with a potassium hydroxide (KOH) solution, imposing an electric current. To keep the flows of hydrogen and oxygen separate, the electrolytic cell has a membrane that allows the transfer of oxydrils between the half-cells but prevents to a certain extent the diffusion of gases, which is known as cross-contamination. Zirfon^{TM} material is currently used as the membrane, but efforts are underway to upgrade it, which is beyond the scope of this paper [4], [5], [6].

The design of control strategies focused on counteracting the gas crossover caused by pressure differences has not been extensively addressed in the literature [7]. Generally, reported control strategies focus on managing the electrolyzer within a network as an electrical consumer and H_2 producer [8], [9]. Control strategies for the outlet valves can only be found in [10], [11]. Although Schug [10] presents a detailed description of an alkaline electrolyzer with experimental results, the control system is not described in-depth. Sánchez et al. [11] report the control of the system pressure with a regulator at the hydrogen outlet and the difference in level with solenoid valves, but the control system is not described in detail. A more in-depth study about the control system aimed to deal with the gas crossover problem is presented in [12]. In this work, the authors propose the design of a control strategy based on the model developed in [13], [14]: an optimal $\mathcal{H}_\infty$ model-based control.

Therefore, the main contribution of this paper is to report the implementation of the $\mathcal{H}_\infty$ optimal controller introduced in [12] and its extensive experimental evaluation in the test-bench described in [13], [14]. The electrolyzer used here as test bench was previously designed and built as a prototype at the Instituto Tecnológico de Buenos Aires (Argentina), making complementary hardware improvements in order to achieve the final objective of maximizing H_2 purity from the mitigation of gas cross-contamination. A more extensive report including a PI controller and a complete comparison assessment of both control strategies can be found in [15].

The remainder of this paper is structured as follows. In Section II, a high-pressure alkaline electrolyzer and the experimental setup are described. The relationship between the final objective of maximizing purity with the intermediate goals of equalizing liquid level and maintaining system pressure is discussed in detail in this section. Section III presents the control design previously developed in [12] and its implementation in the test-bench. An extensive experimental evaluation of the closed-loop system is given in Section IV. Finally, some conclusions are drawn in Section V.

II. Alkaline electrolyzer and its experimental setup

The electrolysis process, which occurs in the electrolytic cell, is represented in Figure 1. Each cell is formed by two electrodes and a membrane that separates both half cells. H_2 and O_2 are formed from water by the application of an electric current I. The differences in pressure and concentration between both half-cells generate a diffusion that must be minimized. A limit of 2% of H_2 in the O_2 stream is accepted, while the lower explosive limit doubles that value (4%, both in air and O_2). Besides, it is desirable to deliver the produced gases at high pressures to reduce the amount of energy consumed in compressing them for storage purposes. The compression of H_2 after its production for gas storage can consume between 10% and 15% of the stored energy. However, the effects of pressure and concentration differences increase at higher pressures. An adequate control

M. David, F. Bianchi and R. Sánchez-Peña are with Instituto Tecnológico Buenos Aires (ITBA), Ciudad Autónoma de Buenos Aires, Argentina. mdavid@itba.edu.ar

F. Bianchi and R. Sánchez-Peña are also with Consejo Nacional de Investigaciones Científicas y Técnicas (CONICET), Ciudad Autónoma de Buenos Aires, Argentina

C. Ocampo-Martinez is with Automatic Control Department, Universitat Politècnica de Catalunya - BarcelonaTECH, Barcelona, Spain

This work has been partially supported by the Spanish projects L-BEST (PID2020-115905RB-C21) funded by MCIN/ AEI /10.13039/501100011033 and MASHED (TED2021-129927B-I00) funded by the European Union - NextGenerationEU (2022UPC-MSC-93823).

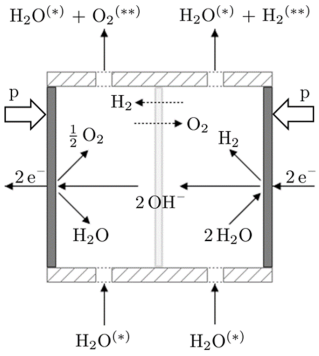

Fig. 1: Scheme of the electrolytic cell with reactions.

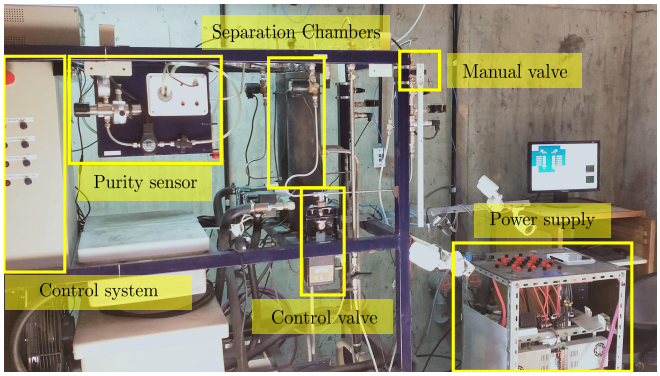

Fig. 2: General photograph of the test setup. In the front side is the O_2 line and in the opposite is the H_2 one.

strategy is able to reduce contamination in order to increase the operating pressure.

In order to analyze different strategies to control the delivery of produced gases, minimizing cross-contamination and guaranteeing the supply pressure, a high-pressure alkaline electrolyzer was designed and built at ITBA. This setup is shown in Figure 2. A detailed description of this experimental platform can be found in [13], [14], [15]. In the pack of 15 alkaline electrolytic cells, H_2 and O_2 are produced from water in a KOH solution environment. Two streams of KOH solution flow from the bottom of the half-cells in order to drag the produced gases bubbles into the separation chambers. There, the bubbles are detached from the solution that is redirected to the cell pack through the action of the recirculation pumps. H_2 and O_2 are accumulated in the upper part of the chamber increasing the pressure of the system. The separation chambers (SCs) are connected to the output lines that are controlled by two motorized valves.

Other auxiliary systems are the equalization line, which connects the bottoms of both SCs in order to equalize solution concentrations, a water injection pump, which refills the water consumed and two heat exchangers, which keep the temperature limited. Pressure sensors are Nagano ADZ-SML 0-250 bar, level sensors are in-house designed capacitance sensors, temperature sensors are PT100, and gas sensors are Shawcity H2-T3HYE and Tx O2 T7OX-V for H_2 and O_2, respectively. The level and temperature variables are digitized by external 24-bit Analog-to-Digital Converters (ADC) ADS1210 and the pressure and gas variables by the internal 10-bit ADC of the MC9S12NE64 microcontroller.

In order to experimentally emulate the storage tanks, two manual valves were added between the electrolyzer and the environment, after the outlet lines. Moreover, a buffer tank was installed before the manual needle valve in order to smooth out changes in outlet pressure which is used as a reference for the control loop. Thus, the measured pressure, which is an input for the controller, is related to both input and output flows, i.e., the openings of the controlled and the manual valves. This solution does not have the same response as a storage tank but allows us to corroborate the operation of the control strategy for similar situations.

Finally, the power supply is a set of switching power supplies that allows a diverse series-parallel configurations to provide a wider range of current and voltage. These power sources work at a constant voltage that can be set to emulate different generation scenarios. In addition, a Pulse Module Width (PWM) control is applied to set intermediate voltages.

Unlike other electrolyzers referred to in the literature with similar setups [10], [16], [11], which operate between ambient pressure and up to 30 bar, the equipment employed here was designed to work up to 200 bar and was tested at a maximum of 60 bar, in this preliminary stage.

III. Control Strategy

This section describes the control strategy proposed in [12] in the test-bench presented in Section II. The control commands two needle-type valves in order to regulate the liquid level difference among the H_2 and O_2 chambers and the resultant pressure within the circuit. Notice that as the electrolyzer works at high-pressure, the contamination problems are more significant.

A. Control scheme

Cross-contamination means that H_2 diffuses into O_2 stream and vice versa. In alkaline electrolyzers, the main crossover is generated in the cell pack where a pressure difference can occur between both half-cells. This phenomenon is illustrated in Figure 1 where H_2 and O_2 cross the membrane. Consequently, the control objective pursues the delivery of H_2 and O_2 at a certain pressure while liquid solution levels in both SCs are kept equalized. This fact is given because a level difference in the SCs produces a pressure difference in the cells due to hydrostatic pressure. In order to meet this requirement, two motorized outlet valves are commanded.

The ranges of operation for electric current I and pressure p are

$$10\ \text{A} < I < 50\ \text{A}, \quad 0\ \text{kPa} < p < 7000\ \text{kPa}. \tag{1}$$

The electrolyzer used for these experiments has an electrode area of $A_{cell} = 143\ \text{cm}^2$. Therefore, the current density J is between 70 and 350 mA/cm^2 under the direct relationship $J = I/A_{cell}$.

In order to have a satisfactory resolution in these operating ranges, and considering the maximum H_2 production of $0.5\ \mathrm{Nm^3/h}$, two needle-type valves were selected for this purpose. The smallest maximum flow coefficient found in the market was used, e.g., $C_v = 0.004$. It is important to note that the pressure in both storage tanks must remain similar in order to control the electrolyzer by installing only one valve per outlet line.

As mentioned before, in standard operation, the objective is to follow the pressure of the storage tanks P_{tank}. A gap must be imposed between the reference pressure P_{ref} set for the control and the current pressure in the tank P_{tank} in order to ensure the outlet flow of produced gases. Moreover, this pressure tracking must be done smoothly to avoid provoking sudden changes in the control actions, which would cause more cross-contamination. In that sense, the reference pressure is defined as

$$P_{\mathrm{ref}} = P_{\mathrm{tank}} + P_{gap}, \text{ subject to } |dP_{\mathrm{ref}}/dt| < \alpha, \quad (2)$$

being α a rate limit in $\mathrm{kPa/s}$. The solution level difference in both SCs is written as

$$\Delta L = L_{\mathrm{H_2}} - L_{\mathrm{O_2}}. \quad (3)$$

This gap should be maintained close to zero in order to keep the pressure at both sides of the membrane equalized. The Zirfon™ membrane is permeable under pressure differences, causing gas crossover [17]. To sum up, by minimizing the level and pressure gaps, the gases produced will have higher purity. Nevertheless, pure gases are not achievable because of the intrinsic diffusion that occurs in this process.

In addition to the outlet valve control, there are several control loops operating simultaneously in an alkaline electrolyzer. Both make-up pump control and refrigeration system control maintain water volume and system temperature, respectively, within a safe operating range. These systems are controlled independently using simple on-off control schemes. A detailed explanation of their operation can be found in [12]. The energy management, i.e., the current-voltage control, is related to the power source and loads. This control is beyond the scope of this work, information on this topic can be found in [18], [19], [20].

As commented in Section II, there is an externally driven DC power supply that is used to emulate changes in electrical current input. The H_2 production is controlled by the outlet valves and is the main topic of this section. All the control loops (i.e., outlet valves, refrigeration system and make-up pump) act independently and simultaneously. For example, when water is injected by the make-up pump, the outlet valves adjust their openings seeking the level equalization. Therefore, the operation of the make-up pump acts as a perturbation to the control loop of the outlet valves.

B. Design of the outlet valve control

The outlet valve control aims to regulate the liquid level difference and the pressure. For this purpose, two control variables values, $u_{\mathrm{H_2}}$ and $u_{\mathrm{O_2}}$, in the range between the minimum (0) and the maximum (10) valve-openings, are set to guarantee that $P_{\mathrm{ref}} - P_{\mathrm{H_2}}$ and ΔL are close to zero.

The design of the outlet valve control is presented in detail in [12]. The first step consists in finding a control-oriented linear model. Thus, the highly-detailed nonlinear model for alkaline electrolyzers reported in [13], [14] with 25 states was reduced to 14 nonlinear states and then linearized at several operating conditions. A set of operating points were selected within the range defined in (1). After comparing the responses of the linear plants and the original model, a single linear model was used to design the controller. The linearization point was established at $p = 4000$ kPa and $I = 30$ A, which represents a typical operation of this electrolyzer. Next, this model was further reduced by truncation of its balanced state-space realization towards a 2nd order LTI model. Its input-output mapping is as follows:

$$\begin{bmatrix} P_{\mathrm{H_2}} \\ \Delta L \end{bmatrix} = G(s) \begin{bmatrix} u_{\mathrm{H_2}} \\ u_{\mathrm{O_2}} \end{bmatrix}.$$

with highly coupled channels. Therefore, $\mathcal{H}_\infty$ optimal control is employed, which also allows considering modelling errors. In this framework, the control specifications are stated as

$$\min_{\text{stabilizing } \tilde{K}(s)} \frac{\|z\|_2}{\|w\|_2}, \quad (4)$$

where z quantifies the tracking error, and w a disturbance or reference. The performance specifications in (4) consider representative signals conveniently weighted [21], [22]. In the case of the electrolyzer, these signals are the pressure regulation around the reference P_{ref} and the level difference ΔL around 0, when changes in the current I and in the reference P_{ref} occur. The control setup is illustrated in Figure 3, where

$$W_e(s) = \begin{bmatrix} k_{e,1} & 0 \\ 0 & k_{e,2} \end{bmatrix}, W_u(s) = \begin{bmatrix} k_{u,1} & 0 \\ 0 & k_{u,2} \end{bmatrix} \frac{10s/\omega_c + 1}{10s/\omega_c + 1},$$

with $k_{e,1} = 0.1$, $k_{e,2} = 4$, $k_{u,1} = 0.8$, $k_{u,2} = 0.8$, and $\omega_c = 0.7$ rad/s being design parameters.

The weighting function $W_e(s)/s)$ penalizes the low frequencies of the pressure and level errors, whilst $W_u(s)$ penalizes the magnitude at high frequencies of the control actions. In Figure 3, the closed-loop setup is presented and the final controller is obtained after solving the optimization problem (4) for $\tilde{K}(s)$ and

$$K_\infty(s) = \frac{1}{s}\tilde{K}(s), \quad (5)$$

as indicated in the same figure. This factorization is needed to ensure the existence of a stabilizing controller. The particular values of the weighting functions W_e and W_u are initially selected by analyzing the bandwidth of model $G(s)$ and the control limitations. The final values are then finely tuned by checking the closed-loop frequency responses.

C. Discrete controller implementation

The controller was discretized at a sampling time $T_s = 0.25$ s and implemented on a Freescale MC9S12NE64 microcontroller. The algorithm was implemented in C language

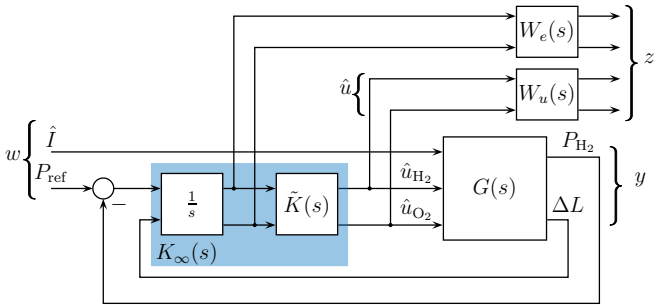

Fig. 3: Control setup for the design of the $\mathcal{H}_\infty$ controller.

considering the system model

$$\begin{aligned} x_{k+1} &= A_z\, x_k + B_z\, e_k, \\ u_k &= C_z\, x_k + D_z\, e_k, \end{aligned} \tag{6}$$

being x_k and x_{k+1} the actual and future states, respectively, e_k are the measured pressure and level errors, and u_k the valves openings. The matrices A_z, B_z, C_z and D_z correspond to the discrete state-space realization of the controller $K_\infty(s)$.

To avoid wind-up problems, a simple conditional integration strategy was implemented. That is, the update of the controller states is switched off when any of the control actions exceed the valve operating range $[0, 10]$.

IV. Experimental Results

This section presents three experimental tests carried out to evaluate the implementation of the previously described control strategy.

A. Increments in the tank pressure

In order to test the proposed controls under a wide range of operating pressure conditions, the manual valves were gradually closed while the electrical current input remained almost constant. With this valve throttling, the pressure could not reach a steady state value. Moreover, the pressure in the buffer tank rises due to the difference in molar flow rates at the inlet and at the outlet. Thus, it was possible to carry out pressure sweeps in a wide operating range.

The closed-loop response of the electrolyzer is presented in Figure 4. The top plot shows the evolution of the electrolyzer pressure P_{H_2} and the buffer-tank pressure P_{tank}. In the test under analysis, the pressure difference was defined as $P_{gap} = P_{\text{tank}} - P_{\text{ref}} = 50\,\text{kPa}$. Figure 4b shows the liquid level in both separation chambers and the difference ΔL, plotted in gray line and associated to the right vertical axis. It can be observed that the controller is capable of tracking the pressure reference P_{ref} and regulating the level difference ΔL around zero.

The control actions, i.e., the valve openings, are shown in Figure 4c. The measures of the level sensors are rather noisy, since they measure the capacitance of a pair of concentric tubes immersed in the solution. In addition, the liquid-free surface does not stay still for two reasons. On the one hand, by the bubbling of the produced gases that rise through the

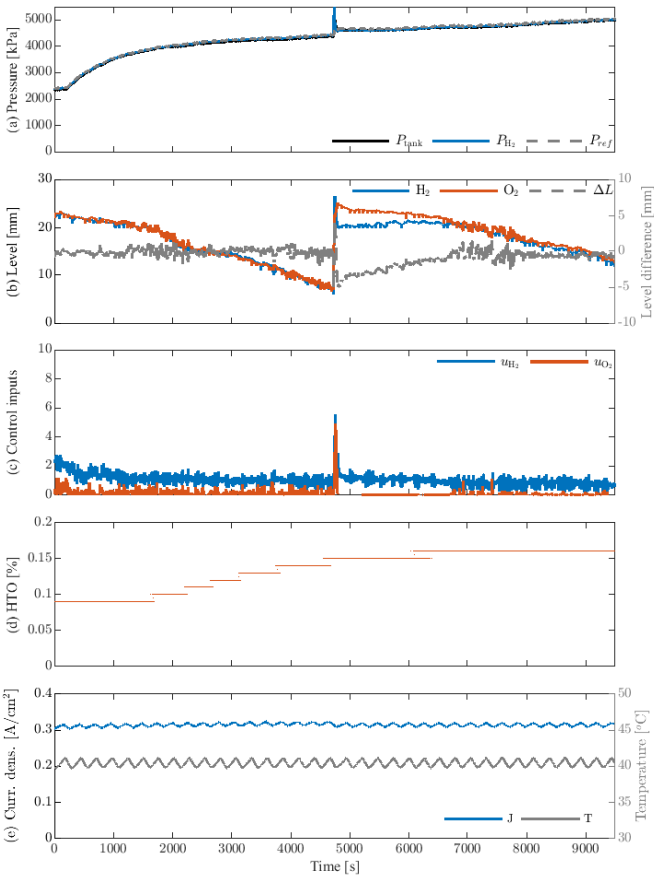

Fig. 4: Experimental closed-loop response using the $\mathcal{H}_\infty$ optimal controller under an increasing tank pressure scenario.

separation chamber and are separated from the solution and, on the other hand, by the recirculation flow imposed by the recirculation pumps. Nevertheless, the $\mathcal{H}_\infty$ controller is able to filter most of the high frequency components. It can also be observed in these and subsequent tests that the O_2 valve operates near the lower limit, which is not entirely desirable. Unfortunately, no other needle valve with smaller opening could be found in the market.

In the electrolytic cells, the diffusion of H_2 towards the O_2 side is always greater than the opposite. For this reason, this value, which is commonly known as HTO (standing for H_2 to O_2), is shown in Figure 4d as a measure of the cross contamination, or similarly, the gas purity. The controller is capable of keeping the cross contamination in low values. However, the contamination increases as system pressure increases. This is because at higher pressures, there is more dissolved gas and therefore more gas diffuses through the membrane. It is necessary to clarify that in the vicinity of the change of the discrete value of HTO, the measurement fluctuates and graphically the points may appear overlapping.

Figure 4e presents the current density in blue line and the temperature in gray line. It can be seen that the cooling system is capable of limiting the temperature around 40 °C without problem. Given this fact and the configuration of

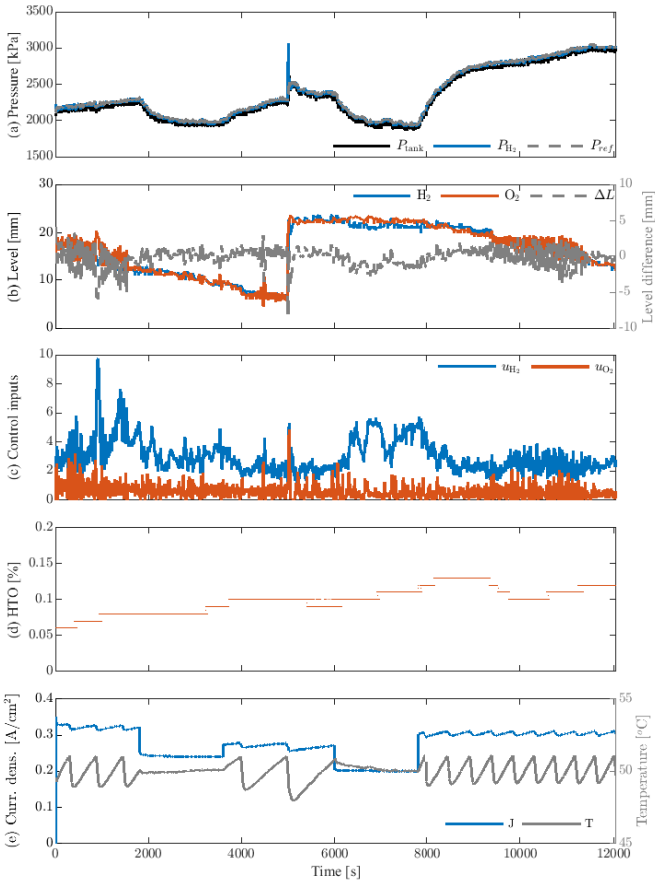

Fig. 5: Experimental closed-loop response using the $\mathcal{H}_\infty$ controller under changes in the electrical current.

the electrical source operating at constant voltage, the electric current remains relatively constant, fluctuating proportionally to the temperature of the system. In case the test would have been carried out at constant current, a decrease in the applied voltage as the temperature increases would have been observed, and vice versa. Moreover, the water injection control loop operates twice in the first test and once in the second one by replenishing the water consumed during the electrolysis process. It is seen in those cases that the levels increase rapidly along with the pressure while the temperature decreases smoothly due to the cold water injected. Since the make-up pump control is independent, the outlet valves control act on this sudden change in the variables as a perturbation, resetting the errors relatively quickly.

B. Changes in the electric current

This test analyzes the behaviour of the proposed control strategy under changes in the electric current. To this end, the current is varied by changing the output voltage of the power supply. Experiments take more than 3 hours with five different values of 95%, 75%, 85%, 65% and 95% of PWM.

The closed-loop response can be seen in Figure 5. As shown in Figure 5a, this test was started with a relatively low tank pressure that rose and fell in accordance with the imposed high or low electrical currents (see Figure 5e). This is because the flow produced is proportional to the current. The mass balance within the buffer tank (see Section II) indicates that the pressure in this tank will vary depending on the difference between the inlet and outlet flows. In this test, the throttling of the manual valve downstream the buffer tank remains constant. Therefore, the output flow depends on the pressure in this tank and, when the gas production increases, the buffer tank pressure grows, and vice versa. In turn, the relationship between the electrical current and gas production implies that the valve openings will be directly related to the current change. However, in this case, as the pressure of the buffer tank also varies with the electrical current, both causes (gas production and pressure reference) compete with each other in imposing the valve opening.

It can be seen in Figure 5e that the operating temperature was set around 50 °C in this test. This response shows that the temperature rises for higher electrical current values forcing to switch-on the refrigeration system. On the contrary, for low values of electric current, the loss of heat to the environment is sufficient so that in the long term the temperature would be below that defined value.

In the HTO evolution shown in Figure 5, two competing causes can be observed. On the one hand, the higher the current, the more gas is produced in each electrode. Therefore, the gas that manages to cross the membrane, in this case H_2, is proportionally diluted in the greater amount of O_2 produced. Besides, the higher the operating pressure, the more contamination there will be due to the nature of the diffusion. Accordingly, contamination fluctuates through the experiments but does not present a clear tendency.

C. Depressurization

The third test analyzed was a significant decrease in the buffer tank pressure. This operation is necessary, for instance, in case the system remains inactive for long periods and it is important to keep the purity high enough for safety reason. During depressurization, the dissolved gas in the alkaline solution gradually separates as the saturation limit decreases. This problem is solved with a slow and controlled action in the opening of the outlet valves.

Figure 6 shows the closed-loop responses corresponding to this scenario. The depressurization is performed by the sudden opening of the manual outlet valve. The time constant observed in the pressure of the buffer tank in Figure 6a is directly related to the tank capacity (volume). Notice that in order to avoid sudden changes in the electrolyzer pressure, there is a limit in the maximum decreasing rate of the pressure reference P_{ref} given by α in (2). For this reason the pressure in the buffer tank falls faster than the electrolyzer pressure P_{H_2}.

In Figure 6c, it can be seen that the $\mathcal{H}_\infty$ controller is able to keep the control action within the limits and avoids saturations that may deteriorate the liquid level regulation. The value of HTO observed in Figure 6d also indicates a satisfactory performance of the $\mathcal{H}_\infty$ controller, as a result of

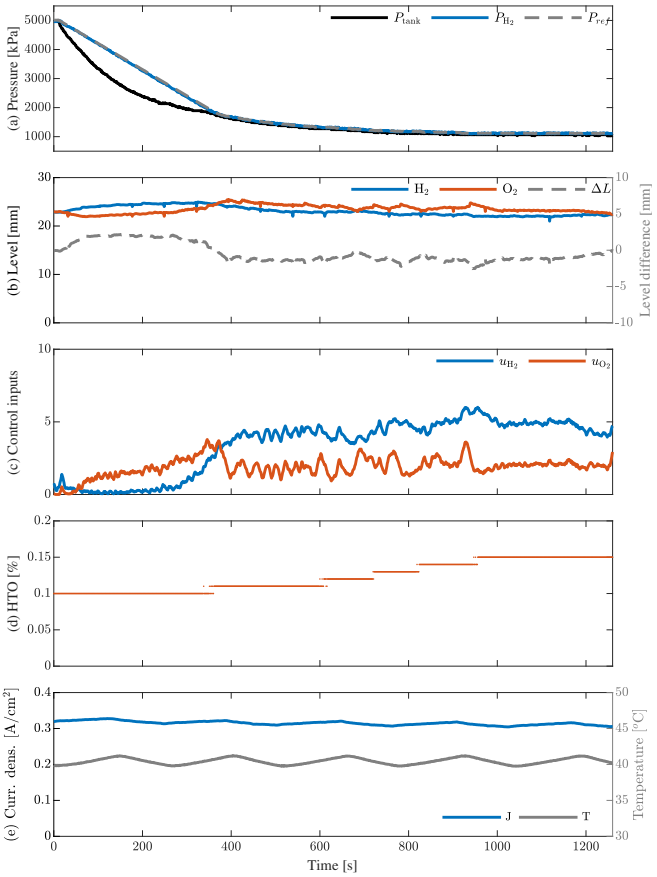

Fig. 6: Experimental closed-loop response using the $\mathcal{H}_\infty$ controller under a sudden opening in the manual needle valve and the consequent decrease in tank pressure.

keeping the valve opening within the limits during the entire test.

In this test, the operating temperature is maintained around 40 °C and the power supply voltage is kept constant, thus the current is almost constant (see Figure 6e).

V. Conclusions

An experimental setup of a high pressure electrolyzer was presented in order to evaluate an $\mathcal{H}_\infty$ optimal control strategy. The tests performed on the prototype electrolyzer allowed to verify the correct operation of the control strategy in different scenarios. In all cases, the contamination was quite below 1% in the O_2 line, which is the one that always presents the greatest contamination given the greater diffusivity of H_2. Finally, the proposed control strategy was capable of minimizing cross-contamination in the produced gases while increasing the system pressure. This action reduces the amount of energy needed to compress the gases for storage purposes. The next step will be to test the prototype electrolyzer at even higher pressure in order to maximize operation. Moreover, further control techniques will be designed and tested over the real setup in order to compare different scenarios and closed-loop control configurations.

References

[1] S. Wang, B. Tarroja, L. Smith Schell, B. Shaffe, S. Scott, Prioritizing among the end uses of excess renewable energy for cost-effective greenhouse gas emission reductions, Appl. Energy 235 (2019) 284–298.

[2] K. Kavadias, D. Apostolou, J. Kaldellis, Modelling and optimisation of a hydrogen-based energy storage system in an autonomous electrical network, Appl. Energy 227 (2018) 574–586.

[3] T. Mahlia, T. Saktisahdan, A. Jannifar, M. Hasan, H. Matseelar, A review of available methods and development on energy storage: technology update, Renewable Sustainable Energy Rev. 33 (2014) 532–545.

[4] H. I. Lee, M. Mehdi, S. K. Kim, H. S. Cho, M. J. Kim, W. C. Cho, Y. W. Rhee, C. H. Kim, Advanced Zirfon-type porous separator for a high-rate alkaline electrolyser operating in a dynamic mode, J. Membr. Sci. 616 (2020) 118541.

[5] P. Trinke, P. Haug, J. Brauns, B. Bensmann, R. Hanke-Rauschenbach, T. Turek, Hydrogen crossover in PEM and alkaline water electrolysis: mechanisms, direct comparison and mitigation strategies, J. Electrochem. Soc. 165 (7) (2018) F502.

[6] M. Schalenbach, W. Lueke, D. Stolten, Hydrogen diffusivity and electrolyte permeability of the Zirfon PERL separator for alkaline water electrolysis, J. Electrochem. Soc. 163 (14) (2016) F1480.

[7] P. Olivier, C. Bourasseau, P. B. Bouamama, Low-temperature electrolysis system modelling: A review, Renewable Sustainable Energy Rev. 78 (2017) 280–300.

[8] F. Vivas, F. De las Heras, A.and Segura, J. Andújar, A review of energy management strategies for renewable hybrid energy systems with hydrogen backup, Renewable Sustainable Energy Rev. 82 (2018) 126–155.

[9] G. Gahleitner, Hydrogen from renewable electricity: An international review of power-to-gas pilot plants for stationary applications, Int. J. Hydrogen Energy 38 (2013) 2039–2061.

[10] C. A. Schug, Operational characteristics of high-pressure, high-efficiency water-hydrogen-electrolysis, Int. J. Electrochem. Sci. 23 (1998) 1113–1120.

[11] M. Sánchez, E. Amores, L. Rodríguez, C. Clemente-Jul, Semi-empirical model and experimental validation for the performance evaluation of a 15 kw alkaline water electrolyzer, Int. J. Hydrogen Energy 43 (2018) 20332–20345.

[12] M. David, F. Bianchi, C. Ocampo-Martinez, R. Sánchez-Peña, Model-based control design for H_2 purity regulation in high-pressure alkaline electrolyzers, J. Franklin Inst. 358 (8) (2021) 4373–4392.

[13] M. David, H. Alvarez, C. Ocampo-Martinez, R. Sánchez-Peña, Phenomenological based model of hydrogen production using an alkaline self-pressurized electrolyzer, in: Proc. of the European Control Conference (ECC), 2019, pp. 4344–4349.

[14] M. David, H. Alvarez, C. Ocampo-Martinez, R. Sánchez-Peña, Dynamic modelling of alkaline self-pressurized electrolyzers: a phenomenological-based semiphysical approach, Int. J. Hydrogen Energy 45 (43) (2020) 22394–22407.

[15] M. David, Mathematical modelling and advanced control design applied to high-pressure electrolyzers for hydrogen production, Ph.D. thesis, Instituto Tecnológico de Buenos Aires - Universitat Politècnica de Catalunya (2021).

[16] P. Haug, M. Koj, T. Turek, Influence of process conditions on gas purity in alkaline water electrolysis, Int. J. Hydrogen Energy 42 (2017) 9406–9418.

[17] M. Schalenbach, A. R. Zeradjanin, O. Kasian, S. Cherevko, K. J. Mayrhofer, A perspective on low-temperature water electrolysis – challenges in alkaline and acidic technology, Int. J. Electrochem. Sci. 13 (2018) 1173–1226.

[18] J. Milewski, G. Guandalini, S. Campanari, Modeling an alkaline electrolysis cell through reduced-order and loss-estimate approaches, J. Power Sources 269 (2014) 203–211.

[19] M. Sánchez, E. Amores, D. Abad, L. Rodríguez, C. Clemente-Jul, Aspen plus model of an alkaline electrolysis system for hydrogen production, Int. J. Hydrogen Energy 45 (2020) 3916–3929.

[20] F.-W. Speckmann, S. Bintz, K. P. Birke, Influence of rectifiers on the energy demand and gas quality of alkaline electrolysis systems in dynamic operation, Appl. Energy 250 (2019) 855–863.

[21] K. Zhou, J. C. Doyle, K. Glover, Robust and Optimal Control, Prentice Hall, 1996.

[22] R. Sánchez-Peña, M. Sznaier, Robust System Theory and Applications, Wiley & Sons, 1998.